Tutor/s

Dr. Sergi Dosta Parras
Departament d'Enginyeria de Materials i Química Física

UNIVERSITAT DE BARCELONA

Grau d'Enginyeria de Materials

Treball Final de Grau

Implementation of bioactive glass coatings obtained by thermal spraying to improve the properties of bone implants.

Implementació de recobriments de vidres bioactius obtinguts mitjançant projecció tèrmica per millorar les propietats en implants ossis.

Alejandro Martín Morata

June 2021

¿Estarías dispuesto a matar hoy a la mitad de la población si con eso pudieras salvar a nuestra especie de la extinción?

Inferno, Dan Brown

Me gustaría agradecer a las persones más cercanas, mis padres y pareja por el apoyo durante los cuatro años de carrera. Me quedo con los compañeros que ahora son amigos y con la cercanía de todos los profesores con nosotros. Principalmente me gustaría agradecer a Bea su esfuerzo, atención y paciencia durante el desarrollo de este trabajo y el tramo final de carrera. También me quedo con el buen rollo del CPT y con la dirección del Dr. Sergi Dosta.

REPORT

CONTENTS

1. SUMMARY

Nowadays human beings stand out for their increased longevity thanks to scientific and technological advances applied to the field of medicine. One of the most important fields is the replacement or repair of bones and body tissues such as a knee operation or a hip prosthesis. Many of these implants are introduced into the body with the addition of a functional ceramic coating such as hydroxyapatite or bioactive glasses like 45S5 which increase the durability of the prostheses and their replacement time.

The main problem that many bioactive glasses suffer comes from their ceramic nature. These materials tend to have a low thermal conductivity, so spraying them becomes a challenge, as they fail to adhere optimally.

This work focuses on increasing the adhesion of 45S5 glass sprayed using the Atmospheric Plasma Spray technique on Ti_4Al_6V substrates using two strategies. The first strategy is to introduce one or more hydroxyapatite interlayers using the demonstrated affinity of HA both 45S5 and substrate in APS. Second strategy, 45S5 agglomerates are produced by using PVA solution to increase the contact area of the particles with the spraying substrate.

The mechanical tensile strength of the coatings is evaluated, and the failure mode is characterized by Scanning Electron Microscopy (SEM) to determine which strategy provides the highest adhesion.

Finally, to complete the work, an in vitro study of bioactivity and biodegradation of the coatings in body fluids simulated medium is performed to evaluate their compatibility.

2. RESUM

Actualment l'ésser humà destaca per l'increment de la longevitat gràcies als avanços científics i tecnològics aplicats al camp de la medicina. Un d'aquest camps més importants és la substitució o reparació de ossos i teixits del cos tals com una operació de genoll o una pròtesi de maluc. Molts d'aquest implants s'introdueixen en el cos amb l'addició d'un recobriment superficial de ceràmics funcionals tals com la Hidroxiapatita o vidres bioactius com el 45S5 que incrementen la durabilitat de les pròtesis i el temps de substitució de les mateixes.

El principal problema que pateixen molts vidres bioactius és la seva naturalesa ceràmica. Aquest materials acostumen a tenir una baixa conductivitat térmica, per la qual cosa projectar-los esdevé un repte, ja que aquests no s'aconsegueixen adherir de manera òptima.

Aquest treball es centra en incrementar l'adherència del vidre 45S5 projectat mitjançant la tècnica de Projecció Tèrmica per Plasma Atmosfèric en substrats de Ti_4Al_6V mitjançant dues estratègies. Primerament es busca introduir una o varies capes intermèdies de hidroxiapatita aprofitant l'afinitat demostrada de la HA amb el vidre i el substrat, mitjançant aquesta tècnica de projecció. En segon lloc es produeixen aglomerats de 45S5 mitjançant una dissolució de PVA amb la finalitat d'aconseguir augmentar l'àrea de contacte de les partícules amb el substrat de projecció.

Posteriorment s'avalua la resistència mecànica a tracció dels recobriment i es caracteritza mitjançant Scanning Electron Microscopy (SEM) el mode de fallada amb la finalitat de determinar quina és l'estratègia que proporciona els majors valors d'adherència.

Per finalitzar el treball es realitza un estudi de bioactivitat i biodegradació dels recobriments en medis de simulació in vitro de fluids corporals per avaluar la seva compatibilitat.

3. INTRODUCTION

3.1 A BIOMATERIALS OVERVIEW

First time someone used a definition for biomaterials was in 1967 by an orthopaedic doctor called J. Cohen. Despite that, it was not until 1974 that a new definition was widely accepted by scientific guild. They stablished that a biomaterial is a systematically, pharmacologically inert substance designed for implantation or incorporation in a living system[1],[2].

These biomaterials are used to replace or enhance any function of human tissues or organs that for any reason have been damaged or undergone degeneration. Currently these materials have acquired a big importance in medicine, and many scientists are working with them within different materials and forms[3].

Contrary as Dr. Cohen said in 1960s, biomaterials research has determined that not only are they inert but also exist active biomaterials. Indeed, current classification of biomaterials includes their bioactivity, biodegradability or biostability properties.

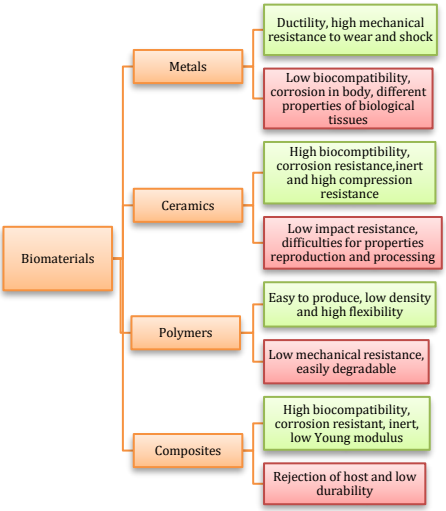

Figure 1: Classification of biomaterials according to the material used and their respective advantages and disadvantages of use[2].

Biomaterials developed from metals, ceramics, synthetic/natural polymers, and natural tissues have been widely used in orthopaedic procedures for decades. Their applicability is determined by its mechanical properties, biodegradation, and surface interaction. For this reason, biocompatibility has become the most important issue in materials research[4].

At present, in 2021, scientists are looking for new materials that solve old problems such as the reduction of some metal prosthesis due to their release of toxic ions, promoting contamination of the human body in addition to reducing mechanical failures or even its weight and infection reactions.

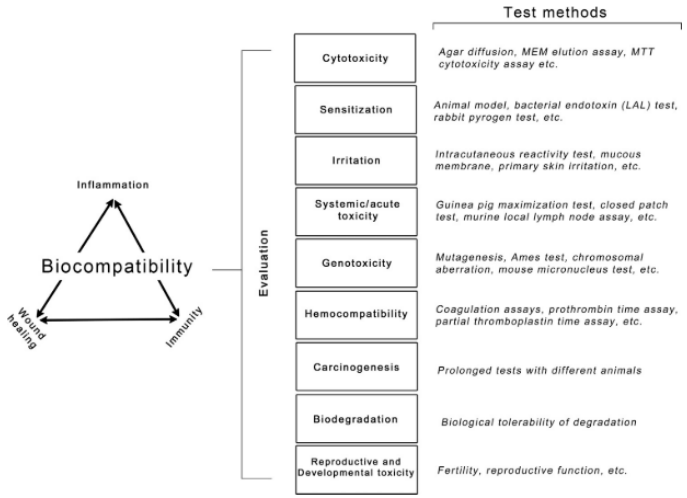

Figure 2: Main biocompatibility aspects and their evaluation methods[4].

Summarizing, biomaterials must be biocompatible and interact with host organism by a proper response on its implantation and presence, reducing adverse effects either on the implant, or inside the organism. They must minimize harmful effects in the area of implantation, nor for other organs or tissues[5], for this reason they must be: blood compatible, nontoxic, noninflammatory, nonpyrogenic, nonallergic and noncarcinogenic[3].

3.1.1. Bioactive Materials

Bioactive materials are an intermediate between resorbable and bioinert, they elicit a specific biological response at the interface of the material when are in contact with body fluids (aqueous solutions). This results in the formation of a bond between the tissues and the material having been favoured by bioactive glasses[6].

Bioactive materials use to classifying in two categories: osseoinductive materials, which interact giving an intercellular and extracellular response, whereas osteoconductive materials only works interacting extracellularly at their interface[7].

3.1.1.1. Bioactive glasses

First bioactive glass appears when Professor Hench decided to make a degradable glass which contains a high calcium concentration. It was in 1969 when Bioglass®, also known as 45S5 bioglass, appears with a composition in the system of SiO_2-CaO-Na_2O-P_2O_5[8]. Bioactive glasses present a similar performance that HA, including properties such as osseoconduction, osseoinduction and osteointegration.

When bioactive glasses are in contact with body fluids they start to dissolve, due to its degradation in aqueous solutions, and release ions such as calcium and phosphate which interact creating an apatite layer in surface helping to regenerate tissues or even bones[6]. For this reason, the main application of bioactive glasses appears in scaffolds or as a filler bone material. A schematic overview of how a bioactive glass works can be seen in Figure 3.

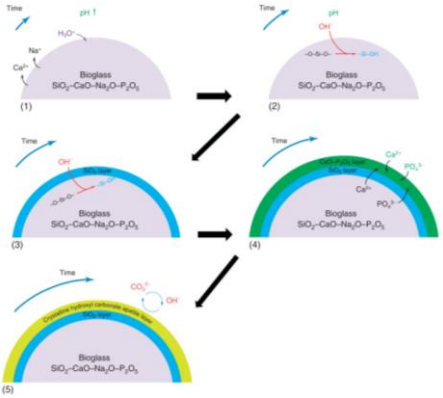

Figure 3: Summary of the sequence of processes occurring at bioactive glass surface[9].

3.1.1.2. Hydroxyapatite

Hydroxyapatite (HA) is considered a phosphate calcium mineral with a chemical $Ca_{10}(PO_4)_6(OH)_2$ but also can be seen in its reduction chemical formulation depending on bibliography[10,11]. HA appears commonly in biomedical field applications due to its bioactive and biocompatibility nature, concretely in bone tissue regeneration enhancing osteogenesis and as a drug delivery material as well[12].

HA became famous due to its similarity to bone composition which is formed by calcium phosphates in 65-70%. Moreover, HA has a good mechanical strength and a porous structure, but the main issue of a wide applicability is caused by its osteoconductive, osseoinductive and osseointegrative properties. For this reason, HA is commonly applicated as coating in hip, knee, or femur prosthesis for example. In addition, not only can HA promote new tissue growth without causing toxicity, inflammation, or any harmful response to host, but also it can be used as a coating on metal implants improving their biocompatibility[13].

3.1.2. Bio coatings

Coatings consist of deposit one or more thin layers in a material's surface using techniques such as thermal spray processes or electrochemical deposition, for example. Coating gets bio when coating material has the aim of improve stability of implants by bonding them to the host bone helping substrate, which normally use to be a metal bioinert prosthesis, to osteointegration in body and inducing a bone regeneration[8].

The aim of deposit a bioactive material as a coating element is enhancing implant performance at early stages by an osseoinductive process around the implant[9].This kind of coating are considered functional coatings and generally biodegradables due to aqueous dissolution in body fluids.

3.2. THERMAL SPRAY

Thermal Spray is usually used as a generic term for describing a group of processes in which metallic and non-metallic materials are deposited as a fine particle in a molten or semi molten condition or even in fully solid state to form a coating in a surface[14]. These processes are grouped in very different ways but normally most of the authors differentiate into three big groups depending on the energy source used to heat the coating material which are chemical by combustion, electrical, including plasma or arc, and kinetics[15].

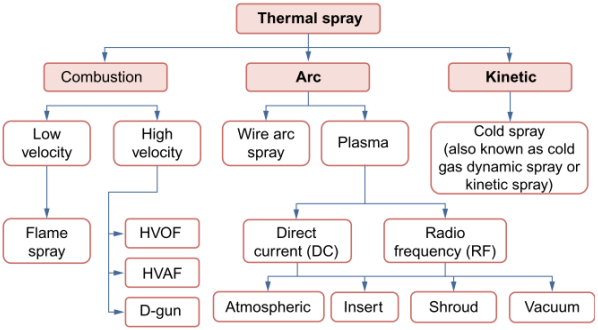

Figure 4: Thermal spray techniques according to the way of accelerating coating element particles[15].

Once the particles are heated, they are accelerated and propelled towards a solid substrate, which is the component to be coated. Material's particles, which could be in powder, wire, or rod form, are accelerate by either process gases or atomization jets until impact the surface. Upon impact, particles and substrate interact forming bonds and causing a thickness build up with a lamellar structure[16].

Thermal spray includes lots of advantages but one of the most interesting is the wide range of materials that could be sprayed including pure metals, metal alloys, hard metals as carbides, oxide ceramics, plastics, cermets, composites, and blended materials[14].

Depending on form, size, material, porosity or mass characteristics, interaction between particles and substrate will vary. Table 1 details some requirements that powders must have to develop a suitable coating. These points also influence in selection of the appropriate thermal spray method, which is principally determined by getting a desired coating material, accomplish with coating performance requirements, embrace a cheap industrialization, and respect part size and portability.

Table 1: Thermal spray powders' requirements[14].

Characteristics	Consequence
Particle size	✓ Suitability to each spray process (20-200 µm) ✓ Reproducible spray properties
Spherical shape of particles	✓ Improved flowability ✓ Uniform melting of powder particles ✓ Clogging-free spraying
Narrow particle size range	✓ Uniform melting of powder particles ✓ High deposition efficiency
Low interparticle porosity	✓ Uniform melting characteristics of powder ✓ Dense coating at low-temperature processes
Manufacturing by mass productions	✓ Appropriate powder price for industrial use

3.2.1. Atmospheric Plasma Spray (APS)

Atmospheric plasma spray has an equipment allowed to operate in atmospheric conditions and also a technique that uses plasma, considered the fourth state of matter which consist of neutral atoms, positive ions and free electrons[16]. Plasma is produced by transferring energy into a gas until the energy level is sufficient to ionize the gas or air, allowing the electrons and ions to act independent of one another. The higher mass ions transfer significantly more kinetics heating energy in the gas than the electrons during collisions. This process due to plasma's high-temperature, makes possible to melt practically everything and all materials including ceramics and refractory metals[14].

As its commented before, APS uses an electrical resource as way of energy for activating and ionize the gas. Normally, this technique requires a big electric arc discharge generated by a powerful direct current (DC) generator capable of producing more than 80 kW. This power is transmitted to the particles through the inert gas which works as a high-velocity gas jet.

For being sprayed, powder's particles must flow and have a typical size range between 10 and 100 µm as starting material[17]. The smaller the particles are, the bigger thermal conductivity will have. Heat penetrates better inside particles depending on its

thermal conductivity and porosity so, fine light particles accelerates and heats quickly; thick dense particles accelerates and heats slower. Once particles have been accelerated and melted or semi-melted, they impact the surface forming a coating.

APS guns use to have a water refrigerator system for reducing temperature gas creates. One of the biggest problems of the guns are gas injection through a small ring, which impart a vortex in the gas. Vortex stabilizes the arc at the cathode tip in the low-pressure region of the vortex and rotates the arc attachment at the anode.

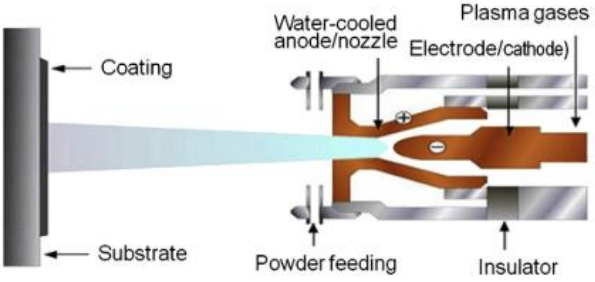

Figure 5: Schematization of APS gun parts and its spreying mechanism[14].

Plasma Spray uses an inert gas that avoid interaction between particles and the jet. Despite that, as now it is known, APS works in atmospheric conditions which normally promotes some interaction between air and powder sprayed particles.

Some articles[14-16], [18], reference that APS can get temperatures nearly 16.000ºC depending on gas composition. Being inert is the principal characteristic the gas must have due to avoid any interaction with powder and gas composition. For this technique, the most used gases are H, Ar and N.

Typical plasma guns use argon combined with a secondary gas to increase energy plasma, related to its ionization potential and thermal heat capacity. Hydrogen has a small molecules size which increase its probability to collision with particles, increasing enthalpy of Ar/He when it is combined with argon. Despite that, this mixture presents an increase of enthalpy that decrease anode/cathode life.

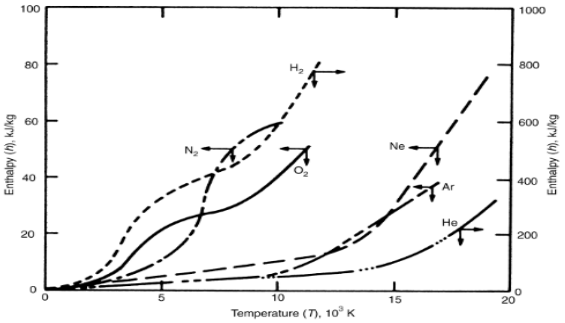

Figure 6: Relation between the enthalpy and temperature of the most commonly used plasma gases[16].

3.3 OBJECTIVES

The aim of this study consists of improving the adhesion strength of the 45S5 bioactive glass coatings produced using Atmospheric Plasma Spray. To achieve this goal two different approaches were considered:

1. Designing different coatings of hydroxyapatite in combination with bioactive glass, taking advantage of the good adhesion of hydroxyapatite with Ti_6Al_4V substrate.
2. Producing agglomerated glass powder, this morphology different from the raw powders favours a greater integration of the molten particles with the substrate.

4. MATERIALS AND METHODOLOGY

4.1 RAW MATERIALS: POWDERS AND SUBSTRATE

Next raw materials have been chosen under the constrain of being biocompatible and perform in specific mechanical and chemical way depending on its functionality inside the body. They also must have, as it is said in previous sections, good resistance to corrosion medium and easy manufacturing on a large scale, always thinking on industrialization.

4.1.1. HA commercial powder

The powder used to obtain HA coatings was CAPTAL 30 from Plasma Biotal Limited (Tideswell, UK).

4.1.2. 45S5 commercial powder

45S5 Bioglass® Powder for produce 45S5 coatings was obtained from Denfotex Research Ltd. (London, UK).

4.1.3. 45S5 agglomerated powder

This agglomerate was formed by adding Polyvinyl alcohol (PVA) as binder to 45S5 milled powder, then a thermal treatment was applied to remove the organic binder.

The grinding conditions were optimised by varying the speed, time, and balls size. Finally, the grinding conditions were 400 rpm for 2 hours using a combination of Ø10 mm and Ø5 mm media.

First, 45S5 was milled at 400 rpm for 2 hours using ball milling PM 400 MA-type from RETSCH® in Y-ZrO_2 vessels ¾ full of Ø10 mm and Ø5 mm as objective to get small

particles inside 20-40 µm range. Once 45S5 was milled, the powder went through sieves of 100-80 and 40 µm particle size. Powder up to Ø100 µm was discarded and the other was collected to combined with PVA solution.

PVA solution preparation consisted of:

1. Warming 150 ml of Milli-Q water until get 50°C at constant agitation with a magnetic stirrer.
2. Add 10 g of PVA little by little because it is difficult to dissolve.
3. Once the 10 g of PVA has been dissolved, it is boiled to ensure complete dissolution. It is then left to stand for 1 h at constant stirring and room temperature.

A glass pestle was used to agglomerate the powders in small parts of 45S5 powder adding small quantities of PVA solution, milling manually for 5 minutes between each addition. Once all powder was semi-wet, it was spread and let rest on paper sheet for 24 hours until it was completely dry. After this process agglomerates were put inside an CRN 4-18 oven from HOBERSAL for 2 hours at 500°C.

4.1.4. Spraying substrates

A Ti_6Al_4V alloy was used as substrates obtained from IBERMETAL S.A. (Spain). Concretely pieces of Ø24,5 mm for Tensile strength test, a 100 x 20 x 5 mm plate was used to metallographic characterization and Ø10 mm and 2 mm thickness discs to biodegradation and bioactivity tests.

Before each spraying, substrates were cleaned with ethanol. After that, they were shot blasted by grade 24 corundom (Al_2O_3) at 5,5 bars keeping each substrate at 45 degrees from vertical to avoid embedded particles on surface. The aim of this is to reach a roughness of 4 µm to assure a god coating adhesion. Finally, samples were cleaned with ethanol again.

4.1.5. Spraying process

The equipment used for Plasma Spray (PS) was A-3000 S model from PLASME TECHNIK and plasma spraying gun PLASME TECHNIK F4-MB model. PS was used to spray four different HA and 45S5 based coatings, represented in Figure 7. The spraying parameters were represented in the table below:

1. Coating formed by 3 HA layers + 2 45S5 layers called Bilayer.
2. Coating formed by a mechanical blend of 50-50% HA-45S5 powder called Blended.
3. Graded 5 layers coating called Graded in the order below:
   - -100% HA
   - -75-25% HA-45S5
   - -50-50% HA-45S5
   - -25-75% HA-45S5
   - -100% 45S5
4. Coating formed by 45S5 agglomerated powder called Agglomerates.

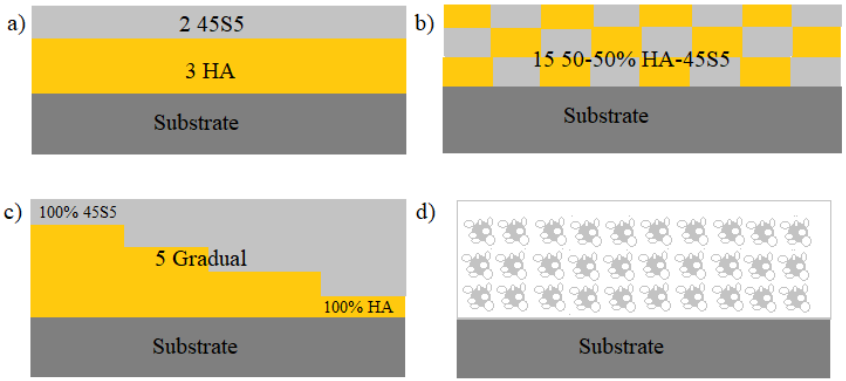

Figure 7: Schematization of the coatings: a) Bilayer b) Blended c) Graded d) Agglomerates.

Figure 8: APS equipment used spraying Ti_6Al_4V substrates.

Table 2: Plasma spray spraying conditions.

Coating	Powder	Ar-H	Work distance (mm)
Bilayer	HA	50-1	80
	45S5	35-12	80
Blended	50-50% HA-45S5	50-1	80
Graded	100% HA	50-1	80
	75-25% HA-45S5	50-1	80
	50-50% HA-45S5	50-1	80
	25-75% HA-45S5	35-12	80
	100% 45S5	35-12	80
Agglomerates	45S5+PVA agglomerates	35-12	80

4.2 Characterization Methods

4.2.1. Powder characterization

To recognise powder, substrate and coatings chemical composition was used an Energy-Dispersive Spectroscopy (EDS) in RÖNTEC detector coupled to scanning electron microscope (SEM) JEOL 5310. Same equipment and Phenom pro-X SEM were also used to characterise powder particles in free surface and its cross section. A sputtering was required to deposit a gold layer onto the samples before observing them

in SEM due to its non-conductor properties. It was used the cathodic pulverization diode POLARON E-5000.

Figure 9: Scanning electron microscope equipment used.

A colorimeter METTLER TOLEDO DSC1 was used to determine binder elimination from 45S5 agglomerates.

Figure 10: Differential Scanning Calorimetry (DSC) equipment used.

4.2.2. Coating characterization

First step to characterise coatings was determining surface roughness evaluated by profilometer MITUTOYO SURFTEST 301 in four different directions as represented in Figure 11. Using the micrometric cutter from BUEHLER ISOMET an accurate small piece was cut to cold mounting preparation using a thermoset resin.

Figure 11: Roughness test directions.

The optical microscopy Leica DMI5000 M was used to analyse coating structure, as well as for measure the thickness. To observe elements distribution of each coating type the mapping option of EDS coupled to SEM was used.

Figure 12: Optical microscope used to analyse samples.

4.2.3. Mechanical coating characterization

Mechanical coating properties were analysed by tensile strength test following ASTM C 633-01 regulation to determine the degree of bonding strength or adhesion grade. This test works with Universal Machine of Mechanical Tests SERVOSIS MCH-102ME. Tests evaluate adherence by applying a traction force in perpendicular direction to substrate until the preparation is broken. This failure can be adhesive if all coating release substrate, cohesive, which indicates that failure happened through coating or even both.

Figure 13: Equipment used to evaluate coatings tensile strength.

Tensile strength test required a previous preparation which consist of adhesion of coated sample to two counter-specimens. Preparation started by adding HTK ULTRA BOND 100® glue (HTK) to contact surfaces. HTK was curing for 2,5 hours at 185°C inside a metal support which contains glued samples keeping them pressed at 14 kN to assure a good adhesion. Once time left, they were unpacked from metal support and filed to eliminate the glue excess in contact interface. Schematic samples preparation can be seen in figure below:

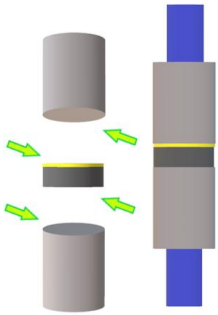

Figure 14: Schematization of tensile strength test preparation to determine coating adhesion.

4.2.4. Biological characterization

Biological characterization was analysed by bioactivity test and degradation test. Weight loss was determined by degradation test submerging each sample in Tris-HCl solution in a concrete volume as a function of sample's area, following rule ISO 10993-14 for identification and quantification of degradation products from ceramics. Tris-HCl solution pH was stabilized at 7,4 by adding HCl 1M. Test keeps a constant temperature of 37°C and a moderate agitation to simulate body environment for 4, 8, 16, 24, 72 and 120 hours.

Samples were weighed by a precision laboratory balance at test starting and ending time to determine the weight loss of the coatings. At each period time studied an amount of solution was collected to be sent for analysis to the ICP-OES laboratory to determine the ions releasing.

Figure 15: Laboratory balance used to weight each sample of this study.

Sample's bioactivity was study at 37°C in thermal isostatic bath "Agibat-20", J.P. SELECTA by immersion in Hank's solution, which is a balanced salt solution used to simulate the body fluids. Test followed rule ISO 23317 for in vitro evaluation for apatite-forming ability of implant materials. The study conditions were active for 3, 7, 14 and 21 days. Each sample was analysed by Phenom pro-X SEM.

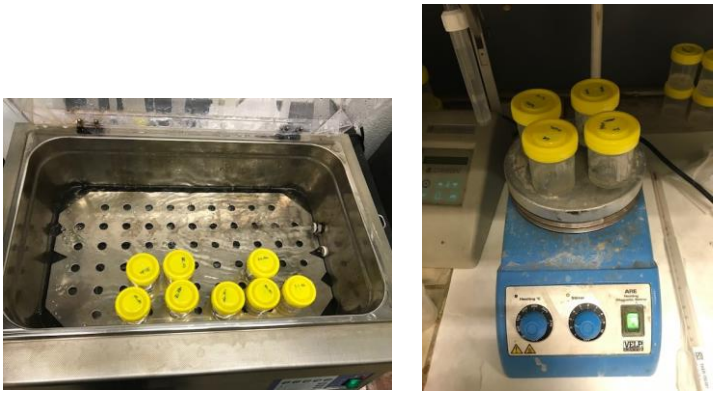

Figure 16: Bioactivity equipment (left), equipment used to degradation test (right).

5. RESULTS DISCUSSION

5.1 POWDER CHARACTERIZATION

5.1.1. Hydroxyapatite CAPTAL 30

HA CAPTAL 30 powders have been observed by checking the technical specifications of the material supplier. The SEM results are consistent, showing homogeneous particles of between 30 - 60 µm with almost perfect spherical geometry. The particles are porous on the surface, so the same can be expected inside.

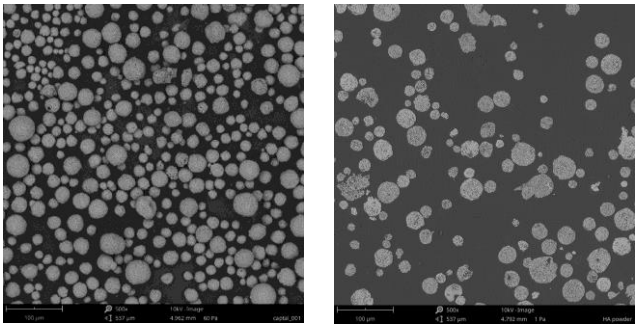

Figure 17: Phenom pro-X SEM micrograph: HA CAPTAL 30 free surface and cross-section at 500x.

To determine this last statement, a study of the cross-section of the particles was carried out, confirming, as can be seen in Figure 17, the high degree of porosity of the particles.

5.1.2. Bioglass® 45S5

From the Bioglass® 45S5, one would expect to see particles between 40 - 60 µm with a much sharper geometry than Hydroxyapatite. The geometry of the particles is cornered with no rounded appearance. Unlike HA, no porosity is observed but compact particles.

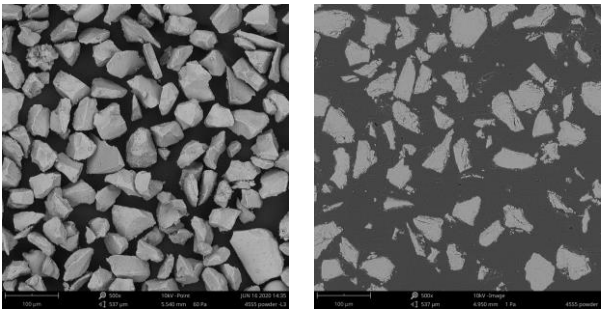

Figure 18:Phenom pro-X SEM micrograph: Bioglass® 45S5 free surface and cross-section at 500x.

Complementing the free-surface micrographs, the cross-section of the glass presented in the Figure 18 still shows these angular geometries. No trace of interior pores is present, confirming the suspicion that the particles are completely solid.

5.1.3. Agglomerates Production

Before forming the agglomerates, it was necessary to grind the 45S5 powder, which initially consisted of particles of between 60 - 40 µm, to a particle size of less than 10 - 20 µm. For this purpose, an initial test was carried out with the ball mill in which two Y-ZrO_2 containers were placed. First one was ¾ filled with Ø10 mm balls and the second with a combination of Ø10 mm and Ø5 mm balls in equal proportions. Then 45S5 powder was introduced until the beads were coated. Grinding was performed for 2 h at 250 rpm.

Once the results shown in Figure 19 were obtained, it was decided to maintain the 2 h time, since the desired results were already obtained. On the other hand, the speed was increased to 400 rpm to further reduce the particle size.

The result was hardly distinguishable but quite representative in terms of fluidity for the case of the mixed ball vessel. Although the particle size did not vary significantly, the powder behaved better after grinding with the ball mix at 400 rpm.

Therefore, it was determined that the ideal conditions for producing 45S5 powder with particle size below 10 µm for agglomeration were to follow the 2 h grinding procedure

at 400 rpm in Y-ZrO_2 vessels ¾ filled with a combination of Ø10 mm beads and Ø5 mm Y-ZrO_2 in equal proportions.

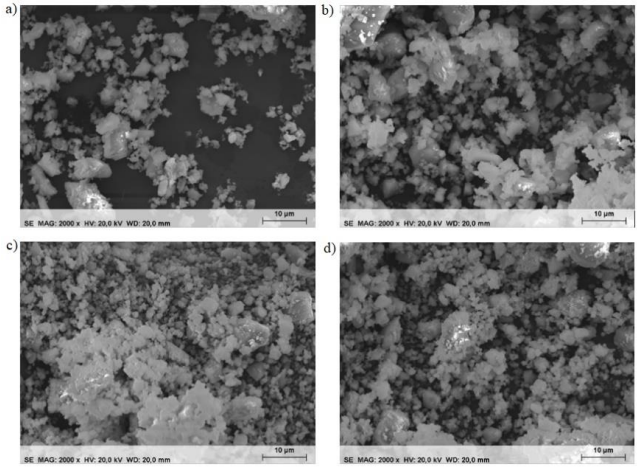

Figure 19: SEM micrograph: a) 45S5 milled for 2 h at 250 rpm with Ø10 mm balls b) 45S5 milled for 2 h at 250 rpm with Ø10 mm and Ø5 mm balls c) 45S5 milled for 2 h at 400 rpm with Ø10 mm balls d) 45S5 milled for 2 h at 400 rpm with Ø10 mm and Ø5 mm balls.

According to literature[19], the PVA solution ratio to achieve HA agglomerates with a particle size between 40 - 63 µm is 0,15 ml/g of powder. Following this reference, it was decided to start with same procedure. The result was a slurry-like paste, so it was decided to increase the dosage. It was tested with 0,250 ml/g, 0,233 ml/g, 0,217 ml/g and 0,200 ml/g until it was obtained a semi-wet solid appearance.

Figure 20: Drying agglomerates in aluminium foil.

The optimum result was set at 0,250 ml/g of powder, thus obtaining, after 1 day of drying, agglomerates with particle sizes between 30 - 50 µm according to SEM images.

If one looks at Figure 21 one can see that the dimensions of the clusters decrease with the reduction in PVA dosage. In the same way, more rounded clusters are obtained with less solution, which is a desirable requirement for powder flowability.

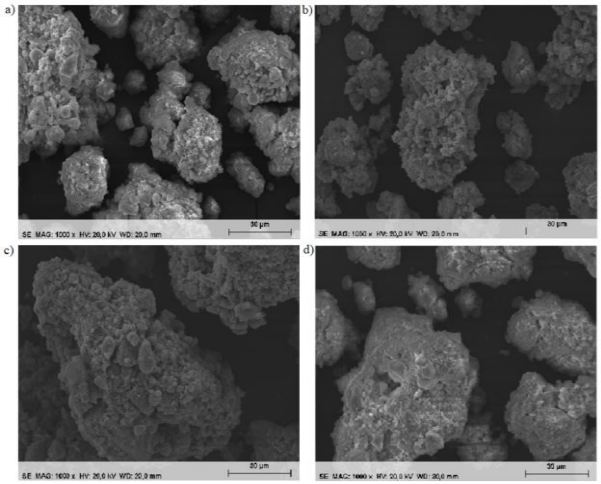

Figure 21: SEM micrograph: 1-day dried agglomerates particles produced by using a) 0,200 ml/g b) 0,217 ml/g c) 0,233 ml/g and d) 0,250 ml/g.

Before applying the heat treatment on the agglomerates, the powder obtained was passed through 80 µm sieve. The aim was to achieve a powder fraction with a size between 40 - 80 µm that meet the spraying conditions of the APS technique.

Finally, a heat treatment was applied to the powders to burnout the binder and obtain the agglomerated powder. For removing the PVA, powders were put into an Al_2O_3 crucible and placed into the furnace. The heating ratio was 10°C/min until 500°C and this temperature was maintained for 1 h. The treatment temperature was chosen to be above the degradation temperature of the PVA and below the glass transition temperature of the bioactive glass, to avoid any phase transformation.

To ensure that the removal of PVA was correct, longer heat treatments were performed in which the powder was kept at 500°C for a longer period. Despite that, the loss mass did not vary after the treatment (7% of weight loss always), therefore the whole process of removal of the organic agent is melted with an hour.

5.1.4. Agglomerates characterization

Figure 21 above shows the free surface agglomerates using Phenom pro-X SEM in the process prior to heat treatment. In this image it can be seen how the particles show a mostly rounded geometry with few vertices despite maintaining the angular particles of the glass.

In contrast, in the images obtained by Phenom pro-X SEM after the 2 h process at 500°C, the geometry is less intuitive. The particles are much more angular and rougher looking with hardly any rounded surfaces. In this case, the small fractions of ground glass are easily observable and form a cluster.

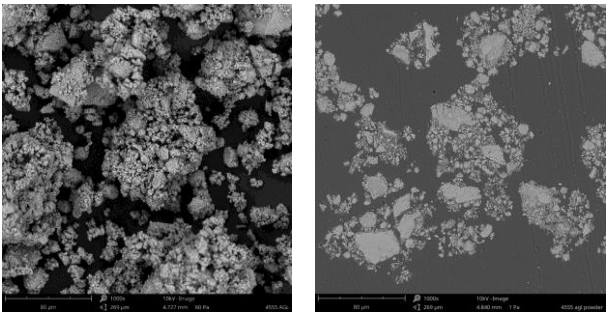

Figure 22: Phenom pro-X SEM micrograph: Free surface and cross-section of 45S5 agglomerate powder after binder elimination at 1000x.

Another observation is the change in appearance, while the particles before the heat treatment were very compact (Figure 21), once the PVA has been eliminated, one can sense a shrinkage or absenting of material. This same observation leads to the intuition, prior to the study of the cross section of the powder, that the particles are going to present a lot of porosity.

To verify the correct removal of all the binding agent in the agglomerates powders a DSC analysis was performed.

First, 45S5 was characterized by calorimetry. The study was carried out for the milled glass after 2 h at 400 rpm. It is observed that two peaks appear, one above 70°C and the other at 100°C. These peaks are rather curious as they do occur, but in a single

peak. However, this is attributed to evaporation losses of surface humidity generated by the environment itself when it is produced or stored. Otherwise, and in line with the bibliography[20], the behaviour of the glass is consistent.

According to the literature[20] the activity of the glass does not start until about 400°C, at which point the OH^- bonds start to break. It also indicates that there is a critical point at 550°C where the glass reaches its T_g value. This point was decisive in the selection of the treatment temperature, as it was a point to avoid exceeding.

Therefore, any alteration in the DSC results before 400°C would correspond to the behaviour of the PVA. As mentioned in different studies[21,22], PVA undergoes a first endothermic reaction at around 78°C corresponding to T_g. Later, at around 230°C it reaches its T_m and from 400°C onwards it starts to degrade, so that with the selected temperature of 500°C we should be able to eliminate any trace of PVA in the particles.

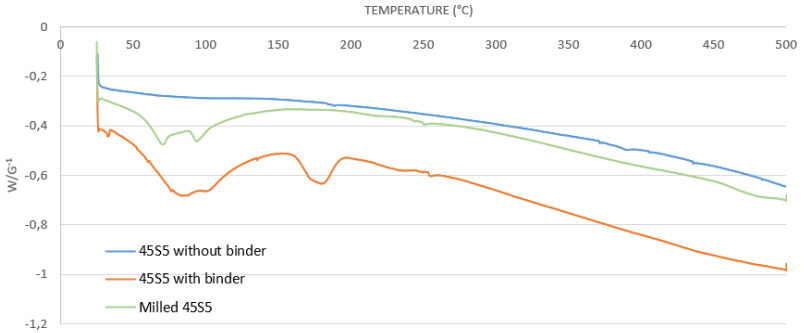

Figure 23: DSC of milled 45S5, 45S5 with binder and 45S5 without binder.

In the resulting curve of the characterised powder without the heat treatment, a small inflection point is observed at 60 - 70°C. This peak is associated with the T_g of the PVA while the peak at 80 - 100°C corresponds to the elimination of surface and crystallised water in the particles. The peak at 180°C is quite different from the main idea of the pure polymer, since in principle it cannot correspond to any reaction other than the melting point. This point is doubtful since the energy produced in the melting point should exceed that of the removal of crystallised water.

The post-treatment curve is observed to be constant and stable until the temperature of 400°C is reached. The result is consistent with expectations and confirms that once the heat is applied to the powder, the PVA has been completely removed from the particles.

Therefore, the selection of the temperature and the application of the treatment on the 45S5 powders has proved to be effective, forming the desired clusters and eliminating any trace of the solution used as a PVA binder.

5.2 SPRAYING RESULTS

5.2.1. Thickness and Roughness

For each type of coating, an initial measurement of the thickness of the sample was made by palmer at the beginning and at the end of each spraying. These records were used as a guideline since the measurement obtained was not very precise. Nevertheless, they helped to verify that the objective of obtaining coatings between 70 - 90 µm was achieved.

Firstly, after completing each spraying, the roughness of the coatings was evaluated in 4 different directions of the specimen. In these measurements it was interesting to know the value of Ra, which is the mean value of the absolute values of the profile heights. At the same time, Rz values were obtained, equivalent to the average of the heights of the peaks and valleys present in the sample.

Table 3: Thickness and roughness for different APS spraying.

Coating	Thickness (µm)	Ra (µm)	Rz (µm)
Bilayer	91,09 ± 12,02	8,38 ± 0,31	41,20 ± 3,64
Blended	62,00 ± 15,71	10,74 ± 0,49	57,38 ± 3,23
Graded	74,87 ± 11,06	9,66 ± 0,71	50,45 ± 3,98
Agglomerates	85,24 ± 23,92	11,10 ± 0,47	60,93 ± 4,28

As can be seen in the Table 3, the values are similar between coatings. This result should not be surprising given that in no case are compositions shared in the spraying. The sample with the most roughness observed appears in the agglomerate coating.

Once the roughness study was completed, a piece was cut using a precision cutter to observe the cross-section of the coatings. The part was cold mounted using resin and a metallographic preparation was done using P600 - P1200 - P2500 silicon carbide abrasive grinding papers.

Using one of the software tools combined with the optical microscope the thickness of the coatings was determined, for this purpose 10 measurements were taken on 3 different areas for each coating. The data shown in Table 3 shows the thickness values of the coatings.

However, the Blended coating does not reach the expected values of 80 µm. This coating posed quite a challenge as it was the one that required the most layers to achieve acceptable palmer measurements. Despite this, as can be seen, the thicknesser partially falls short of the desired requirements. In all cases, the thickness between layers of different materials was evaluated. In these evaluations it was found that there was a great deficiency of HA deposition. On the other hand, the glass layers provided thickness and mass to the sample. Therefore, it is consistent that coatings with higher HA content will respond with lower bulk intuitively due to their low deposition efficiency.

Another point to consider is the spraying conditions for each layer shown in Table 2. For HA deposition, different parameters were used than for 45S5 deposition. As described above, the Graded coating suffered a moment of controversy in layer number 4, consisting of 25 - 75 % HA - 45S5. The conditions used to deposit this layer were those used for the glass due to a higher proportion of the latter in relation to the HA. Prior to that, the deposition behaviour under HA conditions was studied but proved to be low energy compared to glass.

HA is a compound that gives a very good response in APS spraying. The problem arises when this material is sprayed under non-conformal conditions. This is precisely what happens here, in all the tests carried out, layer number 4 underwent a colour change from white to dark grey. This colour change is due to the increase in temperature when the layer is sprayed, as the glass conditions add this factor. As discussed in the following study[23], stoichiometric HA requires a high temperature until it starts to undergo phase changes in its crystalline structure.

The layer that has offered the highest results is the Bilayer layer, reaching values of 90 µm. The most important was not exceed 100 µm with to avoid delamination. In this work we look for similar values so that the study of the different properties were comparative.

5.2.2. Mapping

The study of the distribution of elements was carried out using the EDS detector of the SEM, selecting the main components that formed the coatings. In all cases, Si, Ca, P and Ti were found. Although sodium could be another candidate, it is not present in the analysis images since it simply determined where the 45S5 glass was located. Also, it made mapping difficult to interpretate due to high quantity of colours in picture. By observing the presence of silicon, the distribution of the coating components can already be determined without a problem.

To understand the following images, the composition of the materials must be considered. HA will be recognisable mainly because it has no Si in its structure. On the

other hand, to observe the glass, one must look for red or yellow areas (this is the colour formed by combining the blue of P and the green of Ca) in which silicon appears.

The images below show, in addition to the elements, that these are all porous coatings. The Bilayer coating shows very markedly two layers. A lower one closer to the substrate where the HA is located and a much thicker one formed by the glass on top. The mapping demonstrates the concept of low efficiency in HA deposition. Remembering that there are 3 layers of HA and 2 layers of 45S5, the 3 layers presented a low thickness in comparison with Bioglass®.

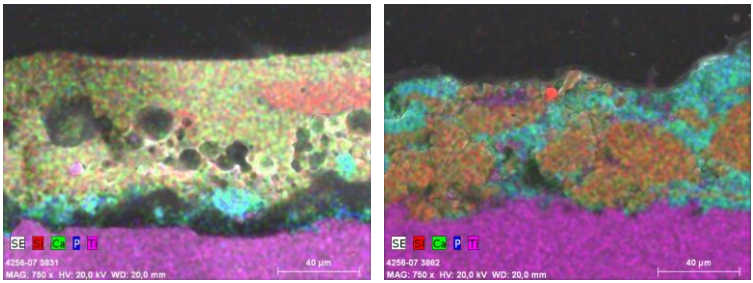

Figure 24: SEM micrograph: Element mapping of Bilayer (left) and Blended (right) coating at 750x.

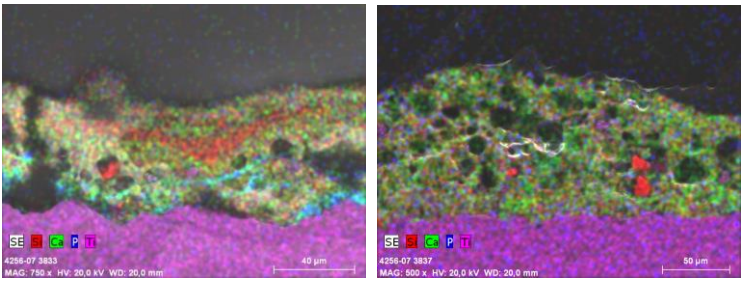

Figure 25: SEM micrograph: Element mapping of Graded (left) and Agglomerates (right) coating at 750x.

In the Blended coating, a good mixture of the two powders can be seen, with Si in different accumulated areas and Ca in others. Therefore, the deposition has been structured in the desired way.

In contrast, Graded coating shows a lower zone of HA, but it is much smaller and not very distinguishable. As you move up the coating you can see the predominance of Si, with HA being much less observable, but you can sense its presence by the dull yellow colour of the glass. As before, little HA presence, again attributed to yield problems.

Agglomerates have no blue zones anywhere on the mapping. This phenomenon is consistent since the blue shades correspond to the HA. A porous but homogeneous coating can be observed throughout the layer.

5.3 TENSILE STRENGTH TEST

The analysis of the mechanical tensile strength of the coatings presented quite interesting data. According to previous studies[24], the strength of a coating completely made of HA had values of 30 MPa. In contrast, resistance values of 8 MPa are given for Bioglass® 45S5 APS coatings.

Depending on the spray material, the minimum accepted value is between 15 and 22 MPa. These values are determined by the ASTM F1147-05: Standard Test Method for Tension Testing of Calcium Phosphate and Metallic Coatings, which accepts values of 15 MPa or more. On the other hand, ASTM F1185-03: Standard specifications for composition of Hydroxyapatite for surgical implants establishes values equal to or higher than 22 MPa.

Two images are shown below for each type of coating tested. The first one shows the specimen projected prior to its preparation for testing. The next image corresponds to the moment after the test has been carried out, visualising the surface resulting from the failure due to the applied stress. The adhesion results are shown in the Table 4.

As can be seen, in most cases a cohesive failure of the coating was observed. The appearance of the surfaces was rough and, in the case of Graded, traces of the glue could be observed, either by absence or excess of glue. This indicated the possibility of

an alteration in the individual results for the tested specimen. However, in this case it did not alter the average result.

Figure 26: Bilayer coating before (left) and after (right) tensile strength test.

Figure 27: Blended coating before (left) and after (right) tensile strength test.

Figure 28: Graded coating before (left) and after (right) tensile strength test.

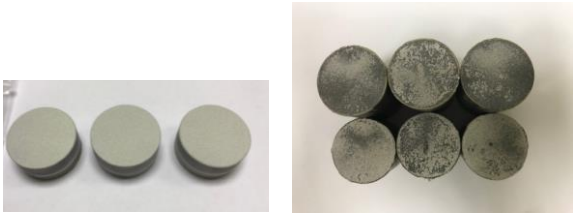

Figure 29: Agglomerates coating before (left) and after (right) tensile strength test.

Table 4: Adhesion values of the tested coating.

Coating	Adherence (Mpa)
Bilayer	19,29 ± 2,25
Blended	22,17 ± 4,68
Graded	11,88 ± 4,05
Agglomerates	12,64 ± 1,99

The total value of Bilayer adherence considers the coating suitable for use although it does not reach the minimum required for implants. This coating showed a cohesive failure mode between the glass layer and the HA layer. In some cases, it can be considered as adhesive failure since the failure occurs between the bond coat and spraying substrate and not through top and bond coat interface. The highlight for this coating is that the adhesion of the 45S5 glass to the Ti substrate has been improved by the HA layer introduced, getting 19,29 MPa.

Tests on the Blended coating gave the best results, making it the only one capable of being used on surgical implants. The value, as with the Bilayer, is completely consistent. The combination of the two materials maintains the strength of the HA and allows the glass to adhere properly.

The breakage at first glance appears to be adhesive, but analysis by EDS mapping shows that the coating comes off, revealing the spraying substrate. Therefore, the failure is caused by an inhomogeneous adhesive/cohesive combination.

Graded and Agglomerates coatings shows the lowest adhesion strength results. Although it is true that a better adhesion was expected in the Graded procedure due to its similarity with Bilayer coating, the result of the Agglomerates has been very positive. As mentioned before, the adhesion strength for 45S5 glass coating was 8 MPa, so in this case this value has been increased by modifying the morphology of the sprayed powders,

improving the results obtained so far. Despite this, it is not possible to reach standardised values for use in medical applications.

In both cases, the breakage of the coating with the naked eye was observed to have occurred through the coating, generating an adhesive failure. This theory was confirmed by a subsequent surface mapping analysis of the specimens in which the deposition substrate was not detected.

5.4 DEGRADATION

For the mass degradation test of the coatings, one specimen of each type was completely immersed for different periods. Before immersion, the samples were weighed and then reweighed after the period of immersion. The total mass loss is due to the dissolution of elements of the coating in the Tris solution. This mass loss was calculated according to the equation:

$$w.l.\% = \frac{m_0 - m_f}{m_0} * 100$$

The results are expressed in Figure 30 as a bar chart organised in four general blocks corresponding to the different coatings. Within each type is the time that each sample was immersed indicating the percentage of mass lost for that fraction of time.

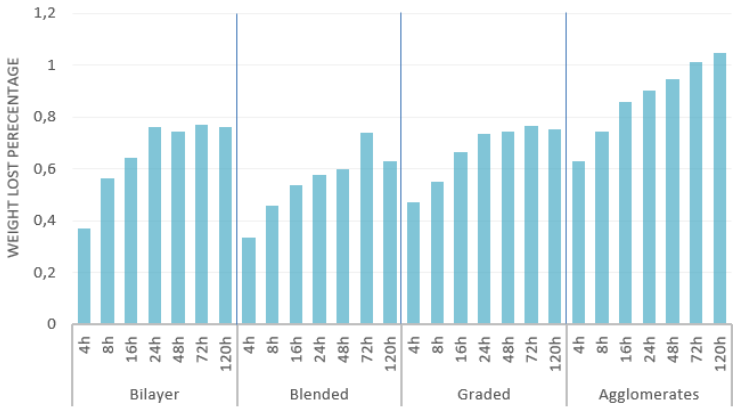

Figure 30: Coating weight lost percentage at 4, 8, 16, 24, 72 and 120 hours.

The data showed increasing values, but with a tendency to stabilise after 72 - 120 h. A current CPT's project results with Bioglass® 45S5 explain that Bioglass® tends to grow to a stable point after 72 h of testing. It is important to relate this trend to the glass because it is the first component in contact with the solution. The fact that it is simply above the HA, and it does not interact with the medium already justifies that the degradation is in line with the behaviour of the glass.

A curious observation is in the Agglomerates coatings. This coating shows the highest percentage of degradation in the medium. This means that, despite having managed to improve adhesion compared to other studies, durability appears as a limiting factor in the application which can be associated with a greater contact area with the fluid. The agglomerates, therefore, will have a shorter service life than any of the other three types of coatings where appear HA.

Another observation was the behaviour of the Blended. These samples were made up of a 50-50 % combination of HA - 45S5 and yet their behaviour was the same as the others. This is due, as mentioned above, to the fact that the glass shows a higher degradation. From these results it could be confirmed that, as there is a higher amount of HA in the system, the durability increases considerably with respect to glass alone.

For this reason, 2 ml were collected from each container in which each sample had been. This analysis, carried out in ICP-OES equipments, shows the quantities of P, Ca, Na and Si dissolved in the solution itself, measured in ppm. Figures 31-34 represent the results of the solution analysis of each specimen.

The Ca contents for the various samples are stable and with values between 80 - 100 ppm, values very similar to those of Na and consistent with the characteristic of being network modifiers. Despite this, higher amounts of Ca were observed in the Graded coating specimens. These results enhance the doubts already presented in the spraying of this same coating. The layer number 4 leads to think that the HA could have changed phase, introducing a higher stoichiometry in calcium than normally.

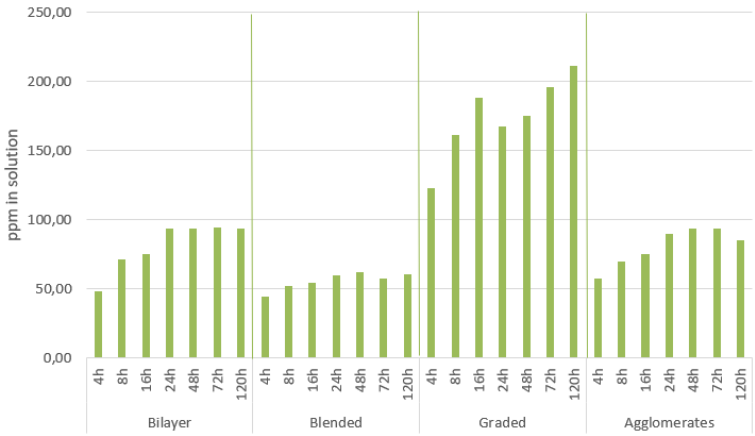

Figure 31: Calcium (Ca) content in solution at 4, 8, 16, 24, 48, 72 and 120 hours.

In the case of phosphorus there was a pattern of immediate growth followed by a drop in concentration after 24 h of testing. This phenomenon, which has also been reported in other studies[25], shows a common trend for this element.

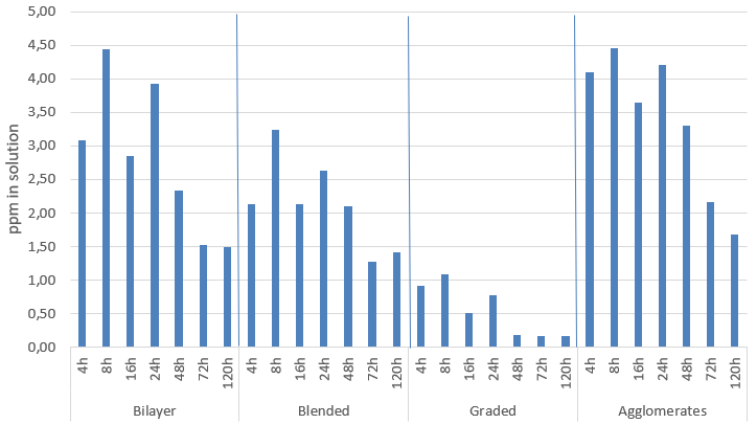

Figure 32: Phosphorous (P) content in solution at 4, 8, 16, 24, 48, 72 and 120 hours.

P is a lattice-forming element, so in principle it should not be easily released from the structure. Phosphorus has a better presence in HA composition than in 45S5. Consistently, the amounts found in solution stand out as the lowest of all the elements analysed. Finding much less P in solution as the study progresses is due to the formation of the natural apatite layer. P continued to be released at the same rate but was consumed in the same proportion to form the apatite layer. If we had continued with more test hours, we would have observed a new upward trend in the amount of P in solution. This ramp results once the natural apatite layer has finished forming.

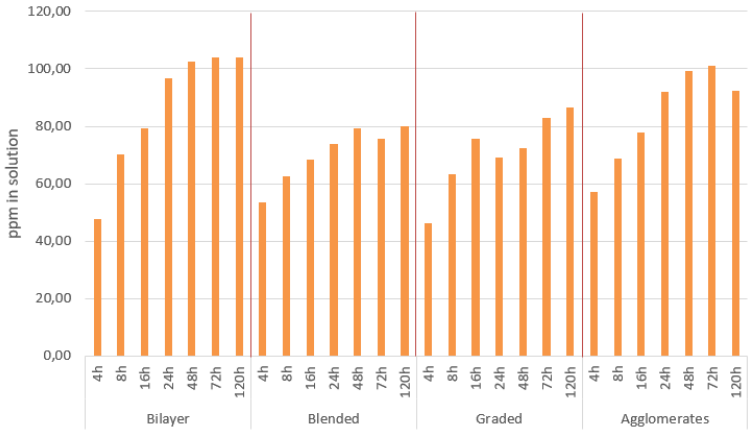

Figure 33: Sodium (Na) content in solution at 4, 8, 16, 24, 48, 72 and 120 hours.

Sodium and Silicon are the main elements in the composition of 45S5 glass. HA is a calcium phosphate in which there is no presence of Si or Na. Therefore, it is assumed that the behaviour of these two ions is directly associated with the behaviour of the glass in relation to the medium.

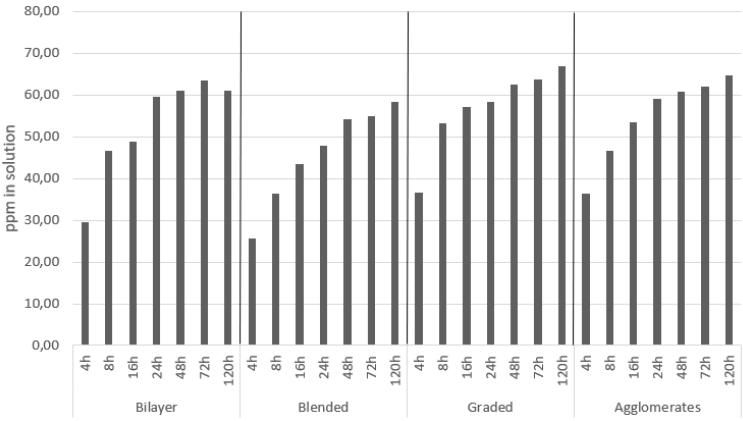

Figure 34: Silicon (Si) content in solution at 4, 8, 16, 24, 48, 72 and 120 hours.

As before, the Na content outweighs the Si content due to its lattice-modifying properties. On the other hand, silicon, which functions as a lattice builder, is more difficult than Na to form ions. For these two elements, only the behaviour of the HA is considered in the Na amounts. This is because it does not contain any silicon in its composition.

5.5 BIOACTIVITY

The bioactivity test was carried out for periods of 3, 7 and 14 under 37°C conditions. Each sample was completely submerged in 10 ml of Hanks' solution maintaining a perpendicular position to the base held by a support piece.

The analysis of the free surface was done in different zones of the specimens because the support itself prevented a complete contact of the coating with the medium. Therefore, the behaviour of apatite nucleation in exposed and unexposed zones was observed. In all the samples, the formation of the natural apatite layer could be seen. According to different studies[23 - 25], there exist three differentiate steps in apatite formation.

In the first stage, a porous surface, and the beginning of the nucleation of small spherical particles were observed. These particles precipitated on the coated surface.

The second stage consisted of a growth of the first particles and the birth of new nuclei. As the immersion time increased, the particle size increased. This growth led to the third stage, where the large number of precipitated particles formed an apatite layer.

This layer could grow continuously, making it a new surface. In this work, it did not exceed 14 days, while another study about HA coating behaviour[29] reports that after three weeks of submersion, this layer acquires a dune-like pattern surface.

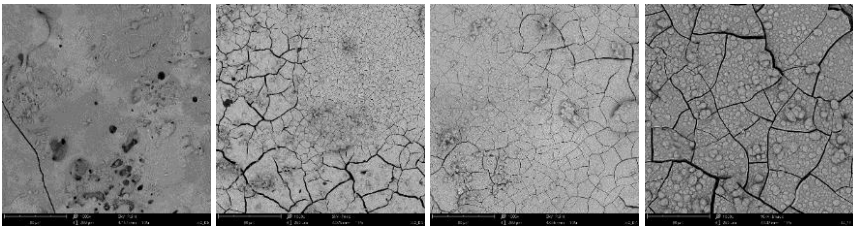

Figure 35: Phenom pro-X SEM micrograph: Natural apatite growing in Bilayer surface at 1000x. Day 0, 3, 7 and 14 from left to the right.

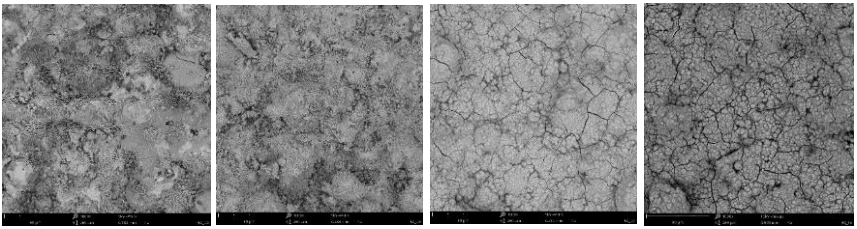

Figure 36: Phenom pro-X SEM micrograph: Natural apatite growing in Blended surface at 1000x. Day 0, 3, 7 and 14 from left to the right.

A common observation is that in all cases the formed layer is heavily cracked. These cracks are caused by drying shrinkage[28], including a stress not accepted by the material. These internal stresses lead to cracking or rupture of the formed surface layer.

If the different coatings are compared, the number of nuclei was higher for Blended and Agglomerates than for the others. When comparing the best coatings, the Blended can be considered as the coating with the highest apatite growth rate. Therefore, a hierarchy in the activity of the coatings can be determined in which Blended and Agglomerates dominate over Bilayer and Graded.

This activity is proportionally related to the glass content in the coating. It is true, however, that in Graded there is apparently also a large presence of 45S5. However, in both Blended and Agglomerates the Bioglass® content is much higher and more concentrated throughout the coating.

This phenomenon means that the presence of 45S5 activates the surface very quickly, inducing the early formation of the natural apatite layer. Nevertheless, all the coatings responded correctly in inducing the formation of the layer. This is finally why all the coatings can be considered bioactive.

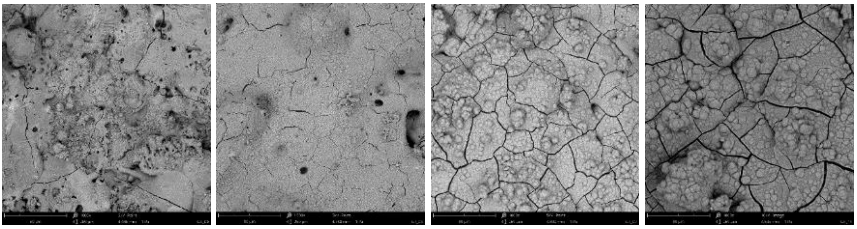

Figure 37: Phenom pro-X SEM micrograph: Natural apatite growing in Graded surface at 1000x. Day 0, 3, 7 and 14 from left to the right.

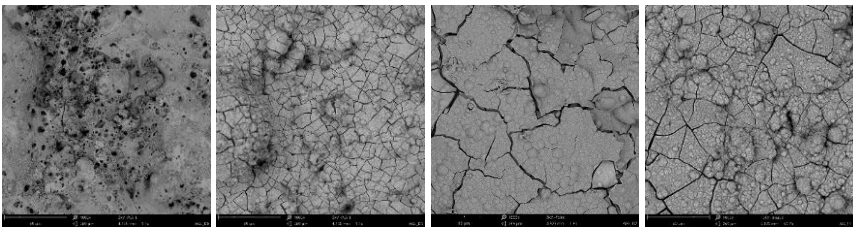

Figure 38: Phenom pro-X SEM micrograph: Natural apatite growing in Agglomerates surface at 1000x. Day 0, 3, 7 and 14 from left to the right.

The cross sections of the coatings at 14 days after submersion in Hanks' solution are shown below. Despite the use of four different strategies, the apatite layer has formed and precipitated in all cases.

It has been previously commented that, at first glance, by means of the free surface images of the coatings, the strategies that gave the greatest growth to the apatite

layer were Agglomerates and Blended. Looking at the cross sections, it is very difficult to determine quantitatively whether this statement is true or not. Apparently, apatite layer precipitated in Graded coating is slightly thinner than in the other three strategies.

While it is true that the thickness is not very comparable, the growth irregularities are differentiated. For the Graded and Agglomerates a flatter and more uniform layer has settled. In contrast, the Bilayer and Blended show an uneven layer with less homogeneous growth. The growth of the layer is determined by the coating itself. If after the spraying it already showed a heterogeneous micrograph, it is to be expected that there are many nucleation points, and the layer keeps the same tendency. A clear example is the micrograph of Graded, a coating that looks like a free-irregularities surface. The apatite nuclei grow in a coordinated manner, generating a practically continuous surface layer.

Despite had all four coating presented a bioactivity, it can be observed that part of the precipitated apatite layer is very cracked and even gives the sensation of detaching. As mentioned above, the generation of cracks is caused by dry shrinkage. The same phenomenon can produce these cracks at the coating-apatite interface, breaking the cohesion of the system formed.

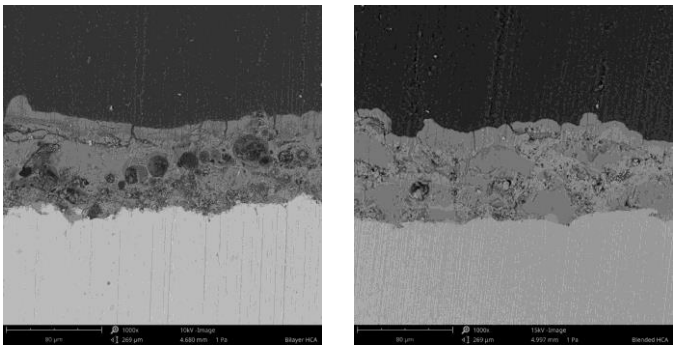

Figure 39: Phenom pro-X SEM micrograph: Cross-section of natural apatite precipitated over Bilayer (left) and Blended (right) Coatings at 1000x.

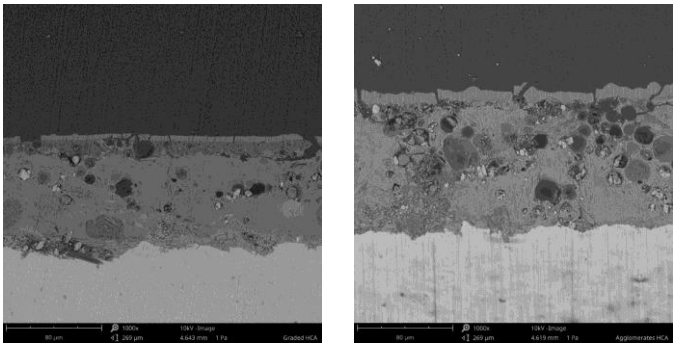

Figure 40: Phenom pro-X SEM micrograph: Cross-section of natural apatite precipitated over Graded (left) and Agglomerates (right) Coatings at 1000x.

6. CONCLUSIONS

The four different deposition strategies of Bioglass® 45S5 on Ti_6Al_4V to improve its adhesion using APS thermal spraying have proven to be successful.

The introduction of HA interlayers between the substrate and the 45S5 powder (Bilayer) has produced a compact, porous, and thick coating. Tensile strength test has shown that it improves the adhesion of the glass in titanium substrates. Its behaviour in simulated media demonstrates its bioactivity, forming the natural apatite layer. Given its level of material loss and in coherence with the requirements for its applicability in bone implants, it is concluded as a suitable strategy for biomedical applications.

The use of blend of HA and Bioglass® presents some difficulties in deposition, resulting in a lower thickness than the desired objective but still acceptable for application. Nevertheless, it is a compact coating that offers the best mechanical performance in terms of adhesion to the substrate. Mapping proves powder is completely mixed in 50-50 % proportions. Moreover, this strategy is the most durable. The precipitation of the natural apatite layer on the coating in simulated media demonstrates its bioactivity. Consistent with the results, optimisation of the powder deposition process would make this candidate the best for biomedical applications.

The Graded scale-up strategy produces a porous and compact coating. EDS mapping characterisation determines heterogeneity in the structure. Although it has the lowest adhesion value, it far exceeds the initial value to be improved. This method shows good durability and, as the Phenom pro-X SEM images show, bioactivity. For this case, in the 4th layer there may have been a phase change in the HA that has caused lower adhesion results than expected. A new Graded-like coating with a modification in this layer could be evaluated in future studies. This strategy does not meet the requirements

for use in implants, so its use in biomedical applications is ruled out until further optimisation.

The production and deposition of the 45S5 glass agglomerate powder generates thick coatings. These coatings have characteristics of compactness, porosity, and homogeneity. It is the most porous coating due to 45S5 powder and could be interesting following this researching line since porosity induces osseointegration. Although it is true that the value of adhesion to the substrate is outside the range of applicability, this is a very optimistic value.

It should be considered that Bioglass® on Ti substrate presents 8 MPa adherence value. In this case, this value is exceeded, thus fulfilling the main objective of the study. Furthermore, performing the lowest durability, the precipitation of the apatite layer establishes this coating as bioactive. Despite the good results obtained, it does not meet the requirements for implants. Optimisation is required for use in biomedical applications.

Finally, this study explain that the presence of HA improves 45S5 adhesion. It is very interesting work in future studies with coatings which combine both materials. The improvement of the mechanical properties provided by HA and the improvement of the biological properties provided by bioglasses can provide technological breakthroughs in biomedical applications.

7. REFERENCES AND NOTES

[1] E. Marin, F. Boschetto, and G. Pezzotti, "Biomaterials and biocompatibility: An historical overview," *J. Biomed. Mater. Res. - Part A*, vol. 108, no. 8, pp. 1617–1633, 2020, doi: 10.1002/jbm.a.36930.

[2] A. Sáenz, E. Rivera, W. Brostow, and V. Castaño, "Ceramic biomaterials: an introductory overview," *J. Mater. Educ.*, vol. 21, no. 5/6, pp. 267–276, 1999.

[3] A. Hudecki, G. Kiryczyński, and M. J. Łos, "Biomaterials, definition, overview," *Stem Cells Biomater. Regen. Med.*, no. ii, pp. 85–98, 2018, doi: 10.1016/B978-0-12-812258-7.00007-1.

[4] S. Ozturk, F. B. Ayanoğlu, M. Parmaksiz, A. E. Elçin, and Y. M. Elçin, *Clinical and surgical aspects of medical materials' biocompatibility*. 2020.

[5] N. Patel and P. Gohil, "A review on biomaterials: scope, applications & human anatomy significance," *Int. J. Emerg. Technol. Adv. Eng.*, vol. 2, no. 4, pp. 91–101, 2012.

[6] D. S. Brauer, "Bioactive glasses - Structure and properties," *Angew. Chemie - Int. Ed.*, vol. 54, no. 14, pp. 4160–4181, 2015, doi: 10.1002/anie.201405310.

[7] L. L. Hench, "Chronology of Bioactive Glass Development and Clinical Applications," *New J. Glas. Ceram.*, vol. 03, no. 02, pp. 67–73, 2013, doi: 10.4236/njgc.2013.32011.

[8] J. R. Jones, "Review of bioactive glass: From Hench to hybrids," *Acta Biomater.*, vol. 9, no. 1, pp. 4457–4486, 2013, doi: 10.1016/j.actbio.2012.08.023.

[9] C. Mas-Moruno *et al.*, "Bioactive Ceramic and Metallic Surfaces for Bone Engineering," *Biomater. Surf. Sci.*, pp. 337–374, 2013, doi: 10.1002/9783527649600.ch12.

[10] S. Pai, S. M Kini, R. Selvaraj, and A. Pugazhendhi, "A review on the synthesis of hydroxyapatite, its composites and adsorptive removal of pollutants from wastewater," *J. Water Process Eng.*, vol. 38, no. August, p. 101574, 2020, doi: 10.1016/j.jwpe.2020.101574.

[11] N. A. S. Mohd Pu'ad, R. H. Abdul Haq, H. Mohd Noh, H. Z. Abdullah, M. I. Idris, and T. C. Lee, "Synthesis method of hydroxyapatite: A review," *Mater. Today Proc.*, vol. 29, no. November 2018, pp. 233–239, 2019, doi: 10.1016/j.matpr.2020.05.536.

[12] A. Haider, S. Haider, S. S. Han, and I. K. Kang, "Recent advances in the synthesis, functionalization and biomedical applications of hydroxyapatite: a review," *RSC Adv.*,

vol. 7, no. 13, pp. 7442–7458, 2017, doi: 10.1039/c6ra26124h.

[13] D. S. Gomes, A. M. C. Santos, G. A. Neves, and R. R. Menezes, “A brief review on hydroxyapatite production and use in biomedicine,” *Ceramica*, vol. 65, no. 374, pp. 282–302, 2019, doi: 10.1590/0366-69132019653742706.

[14] P. Vuoristo, *Thermal Spray Coating Processes*, vol. 4. Elsevier, 2014.

[15] M. Ghosh, A. Roy, A. Ghosh, H. Kumar, and G. Saha, *Antibacterial and antimicrobial coatings on metal substrates by cold spray technique: Present and future perspectives*. Elsevier Inc., 2020.

[16] A. J. Sturgeon, *Thermal spray technology*, vol. 1, no. 6. 1993.

[17] H. Kassner, R. Siegert, D. Hathiramani, R. Vassen, and D. Stoever, “Application of suspension plasma spraying (SPS) for manufacture of ceramic coatings,” *J. Therm. Spray Technol.*, vol. 17, no. 1, pp. 115–123, 2008, doi: 10.1007/s11666-007-9144-2.

[18] E. Bakan and R. Vaßen, “Ceramic Top Coats of Plasma-Sprayed Thermal Barrier Coatings: Materials, Processes, and Properties,” *J. Therm. Spray Technol.*, vol. 26, no. 6, pp. 992–1010, 2017, doi: 10.1007/s11666-017-0597-7.

[19] R. Emilia *et al.*, “Ag-doped HA coatings for biomedical applications deposited by cold spraying,” 2017.

[20] D. Bellucci, V. Cannillo, and A. Sola, “An overview of the effects of thermal processing on bioactive glasses,” *Sci. Sinter.*, vol. 42, no. 3, pp. 307–320, 2010, doi: 10.2298/SOS1003307B.

[21] F. Reguieg, L. Ricci, N. Bouyacoub, M. Belbachir, and M. Bertoldo, “Thermal characterization by DSC and TGA analyses of PVA hydrogels with organic and sodium MMT,” *Polym. Bull.*, vol. 77, no. 2, pp. 929–948, 2020, doi: 10.1007/s00289-019-02782-3.

[22] S. Baklouti, J. Bouaziz, T. Chartier, and J. F. Baumard, “Binder burnout and evolution of the mechanical strength of dry-pressed ceramics containing poly (vinyl alcohol),” *J. Eur. Ceram. Soc.*, vol. 21, no. 8, pp. 1087–1092, 2001, doi: 10.1016/S0955-2219(00)00305-8.

[23] K. A. Gross and C. C. Berndt, “Thermal processing of hydroxyapatite for coating production,” *J. Biomed. Mater. Res.*, vol. 39, no. 4, pp. 580–587, 1998, doi: 10.1002/(SICI)1097-4636(19980315)39:4<580::AID-JBM12>3.0.CO;2-B.

[24] M. G. Latorre, “Recubrimientos de hidroxiapatita obtenidos mediante proyección térmica por plasma atmosférico,” in *Recubrimeintos biocompatibles obtenidos por Proyección Térmica y estudio in vitro de la función osteoblástica*, 2007.

[25] Q. Zhang, J. Chen, J. Feng, Y. Cao, C. Deng, and X. Zhang, “Dissolution and mineralization behaviors of HA coatings,” *Biomaterials*, vol. 24, no. 26, pp. 4741–4748, 2003, doi: 10.1016/S0142-9612(03)00371-5.

[26] Y. W. Gu, K. A. Khor, and P. Cheang, "In vitro studies of plasma-sprayed hydroxyapatite/Ti-6Al-4V composite coatings in simulated body fluid (SBF)," *Biomaterials*, vol. 24, no. 9, pp. 1603–1611, 2003, doi: 10.1016/S0142-9612(02)00573-2.

[27] S. W. K. Kweh, K. A. Khor, and P. Cheang, "An in vitro investigation of plasma sprayed hydroxyapatite (HA) coatings produced with flame-spheroidized feedstock," *Biomaterials*, vol. 23, no. 3, pp. 775–785, 2002, doi: 10.1016/S0142-9612(01)00183-1.

[28] Y. W. Gu, K. A. Khor, D. Pan, and P. Cheang, "Activity of plasma sprayed yttria stabilized zirconia reinforced hydroxyapatite/Ti-6Al-4V composite coatings in simulated body fluid," *Biomaterials*, vol. 25, no. 16, pp. 3177–3185, 2004, doi: 10.1016/j.biomaterials.2003.09.101.

[29] X. Zhou, *Hydroxyapatite/Titanium Composite Coatings for Biomedical Applications*. 2012.